Quasi 2-D Field Reconstruction Using the Conjoint Cylindrical Wave Expansion

Ryan J. Pirkl, *Student Member, IEEE*, and Gregory D. Durgin, *Senior Member, IEEE*

***Abstract*—Off-the-horizon propagation severely degrades the accuracy of any field reconstruction technique that presupposes a two-dimensional (2-D) wireless channel. Therefore, employing the 2-D cylindrical wave expansion (CWE) to interpolate perimeter channel measurements into a planar region often yields poor results. Here, the CWE is adapted for real-world radio channel measurements by selectively combining the basis functions from two similar CWEs. Using both simulated and experimental measurement data, it is shown that this conjoint CWE yields a more accurate reconstruction than the conventional CWE yet requires no additional measurements. Thereby, this field reconstruction-based channel imaging technique will enable more complete investigations of the wireless channel's spatial behavior and allow researchers to isolate and characterize the actual mechanisms underlying radio wave propagation.**

***Index Terms*—Channel imaging, cylindrical wave expansion, field reconstruction, wireless channel measurements.**

I. Introduction

ALTHOUGH radio wave propagation is inherently a three-dimensional (3-D) phenomenon, the composition and geometry of wireless channels often justify a more simplified two-dimensional (2-D) representation wherein the majority of power is propagated along the horizon at a 0° elevation angle. According to the uniqueness theorem of electromagnetics, for such 2-D wireless channels composed solely of transverse electric (TE) or transverse magnetic (TM) fields, a set of coherent channel measurements along the perimeter of a planar region will enable an exact reconstruction of the channel within the region. In practice, however, the accuracy of a 2-D field reconstruction will depend on the accuracy of the underlying 2-D channel approximation. An early investigation of elevation angle of arrival (AoA) in wireless channels by Lee and Brandt concluded that "signal arrival is concentrated in elevation angles lower that 16°" [1]. More recent measurement campaigns utilizing sophisticated phased arrays have reached similar conclusions [2]–[6].

In what is perhaps the most complete measurement campaign to-date, Kalliola *et al.* found that, when averaged over a variety of wireless channel environments, vertically polarized antennas yielded a mean elevation AoA of 4.4° and a standard deviation of 9.0°. A horizontally polarized receive antenna increased the mean and standard deviation to 7.5° and 14.7°, respectively [7]. For power-based descriptions of wireless channels, such small elevation angles lend strong support to the 2-D channel approximation. However, it is unclear if the complex time-harmonic electric field may also be approximated as 2-D. The sensitivity of phase to small spatial changes suggests that, even for small elevation AoA clustered about the horizon, a strictly 2-D model of the wireless channel might lead to an inaccurate description of the field's complex phasors. Thereby, one might expect that small elevation AoA would also degrade the accuracy of any 2-D field reconstruction technique.

This paper examines the reconstruction accuracy of the 2-D *cylindrical wave expansion* (CWE) when applied to coherent wireless channel measurements along a pair of concentric closed contours. It is shown that even for small elevation AoAs, the reconstruction error of the conventional CWE can be significant, especially for large measurement regions. To compensate for the possibility of nonzero elevation AoAs, we develop the *conjoint* CWE, which combines the basis functions from a pair of CWEs with slightly different wavenumbers via the singular value decomposition (SVD). As shall be shown, the conjoint CWE produces a more accurate reconstruction in so-called *quasi-2-D* wireless channels without requiring any additional measurement data. Thereby, the conjoint CWE offers an accurate reconstruction-based channel imaging technique that may be used for studying the spatial characteristics of real-world wireless channels. The resulting channel image may even be processed using various digital image processing techniques so as to extract and examine the individual propagation mechanisms contributing to the wireless channel in the measurement region. This method of analysis is both more versatile and more complete than current investigative techniques, which rely on directional antennas or array beamforming to measure power incident from select azimuth AoAs [8]–[13]. Discussion begins with a review of the conventional CWE for 2-D electromagnetic fields. This is followed by a qualitative analysis of the quasi-2-D fields resulting from plane waves propagating at small elevation angles with respect to the horizon. The conventional CWE is then adapted to provide a more accurate field reconstruction in these quasi-2-D fields. The resulting conjoint CWE is studied and validated analytically as well as empirically using actual measurement data.

II. Cylindrical Wave Expansion

Let us assume a 2-D electromagnetic field that is invariant in the z-direction. Without loss of generality, we restrict our analysis to the z-component of a time-harmonic electric field,

Manuscript received February 12, 2008; revised September 10, 2008. Current version published April 08, 2009. This work was supported by the National Science Foundation under a Graduate Research Fellowship.

The authors are with the Propagation Group, School of Electrical and Computer Engineering, Georgia Institute of Technology, Atlanta, GA 30332 USA (e-mail: rpirkl@gatech.edu; durgin@ece.gatech.edu).

Color versions of one or more of the figures in this paper are available online at http://ieeexplore.ieee.org.

Digital Object Identifier 10.1109/TAP.2009.2015803

denoted $E_z(\rho,\phi)$ in cylindrical coordinates. Within a homogeneous and source-free medium, $E_z(\rho,\phi)$ may be expanded as a summation of cylindrical waves according to [14]

$$E_z(\rho,\phi)=\sum_n a_n J_n(k\rho)e^{jn\phi} \tag{1}$$

where $J_n(x)$ is the nth order Bessel function of the first kind, a_n is the nth term's coefficient, and k is the time-harmonic field's wavenumber given by

$$k=2\pi/\lambda \tag{2}$$

where λ is the wavelength of the time-harmonic field within the medium. From the uniqueness theorem, it is known that for a lossy medium, knowledge of E_z along any closed contour Γ allows for perfect reconstruction of E_z within the region Ω bounded by Γ [14]. Thereby, it is possible to uniquely determine all a_n from a *single* closed contour. While theoretically sound, numerical solutions for a_n based on E_z along a single contour result in an electric field that is dominated by the resonant modes of the region's geometry [15]. Using only the electric field, one may suppress these resonant modes through the *dual-surface* approach, which augments the original closed contour Γ with an additional contour Γ', concentric to and approximately $\lambda/4$ within Γ [16], [17]. Thus, for practical applications, the CWE will require knowledge of the electric field along at least *two* concentric closed contours interspaced by $\lambda/4$.

III. Quasi-2-D Electromagnetic Fields

The conventional CWE is only intended for the canonical case of true 2-D fields. Therefore, care must be taken when appying this 2-D expansion to the 3-D fields encountered in the real world. Even so-called 2-D wireless channels will exhibit small variations in the z-direction due to plane waves' propagating at nonzero elevation angles. Consider a single homogeneous plane wave with amplitude E_0 and wavevector $\bar{k}$ given by

$$\bar{k}=k\cos\alpha\cos\beta\hat{x}+k\cos\alpha\sin\beta\hat{y}+k\sin\alpha\hat{z} \tag{3}$$

where k is again the wavenumber of the time-harmonic plane wave. The z-component of the electric field due to this plane wave is given by

$$E_z(\bar{r})=E_0e^{-j\bar{k}\cdot\bar{r}} \tag{4}$$

where $\bar{r}$ is the observation point given by

$$\bar{r}=\rho\cos\theta\cos\phi\hat{x}+\rho\cos\theta\sin\phi\hat{y}+\rho\sin\theta\hat{z}. \tag{5}$$

Fig. 1(a) and (b) defines the real components of the spherical angles α,β,θ, and ϕ. Note that the elevation angles α and θ are defined with respect to the xy-plane to facilate discussion of elevation AoA with respect to the horizon. For the scalar field $E_z(\bar{r})$ to be invariant in z and truly 2-D, the z-component of $\bar{k}$ must be zero. Thereby, any $\bar{k}\cdot\hat{z}\neq 0$ and, more specifically, any $\alpha\neq 0$ will result in a field with variations in the z-direction. We are primarily interested in α that lead to an *approximately* 2-D wireless channel. In loose, qualitative terms, we define the corresponding *quasi-2-D* fields as those whereby all contributing plane waves have a small, purely real α, bearing in mind that "small" is roughly within $\pm 16^\circ$, as is often the case for real-world wireless channels. Note that by requiring that α be purely real, we eliminate the possibility of an E_z whose amplitude is exponentially decaying in the $\pm z$-direction.

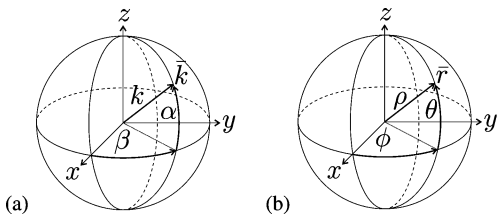

Fig. 1. Coordinate systems: (a) wavevector $\bar{k}$ and (b) observation point $\bar{r}$.

IV. A Modified Expansion for Quasi-2-D Fields

Using (3) and (4), the electric field on the plane $z=0$ due to an arbitrary plane wave may be expressed in cylindrical coordinates as

$$E_z(\rho,\phi,z=0)=E_0e^{-jk\rho\cos\alpha[\cos\beta\cos\phi+\sin\beta\sin\phi]} \tag{6}$$

which simplifies to

$$E_z(\rho,\phi,z=0)=E_0e^{-jk\rho\cos\alpha\cos(\beta-\phi)}. \tag{7}$$

Using the expansion

$$e^{-j\rho\cos\theta}=\sum_n J_n(\rho)e^{-jn(\theta+\pi/2)} \tag{8}$$

and simplifying, (7) may be rewritten as

$$E_z(\rho,\phi,z=0)=E_0\sum_n e^{-jn(\beta+\pi/2)}J_n(k\rho\cos\alpha)e^{jn\phi}. \tag{9}$$

Observe that the conventional CWE described in (1) is a special case of (9) whereby $\alpha=0$ and $a_n=E_0e^{-jn(\beta+\pi/2)}$. Thus, (9) suggests a more general α-dependent CWE of the form

$$E_z(\rho,\phi,z=0)=\sum_n a_nJ_n(k\rho\cos\alpha)e^{jn\phi}. \tag{10}$$

Comparing the conventional CWE in (1) and the α-dependent CWE in (10), we note that (10) is equivalently a CWE for a 2-D electric field with a wavenumber given by $k\cos\alpha$. Thus, to create an expansion for quasi 2-D fields, we could simply combine the basis functions from multiple α-dependent CWEs provided that their corresponding α are small. Thereby, let us define a new *conjoint* CWE that combines the basis functions

from $M\alpha$-dependent CWEs, each with a specific wavevector elevation angle α_m. The conjoint CWE may then be written as

$$E_z(\rho,\phi) = \sum_{m=1}^{M} \sum_{n} a_{mn} J_n(k_m \rho) e^{jn\phi} \tag{11}$$

where a_{mn} are the unknown coefficients and $k_m = k\cos\alpha_m$ is the α-dependent wavenumber corresponding to the mth α-dependent CWE. Let us assume that the set of wavenumbers $\{k_m\}$ is described by a uniform discretization of $k\cos\alpha$

$$k_m = k - \Delta\pi(m-1) \text{ for } m = \{1,2,\ldots,M\} \tag{12}$$

where Δ is the *wavenumber stepsize*. Thereby, the largest allowable k_m corresponds to the electric field's actual wavenumber k. When $M = 1$, (11) is identical to the conventional CWE given in (1). Lastly, note that from a system-of-equations standpoint, the case of $M = 2$ may be solved uniquely using the same two $\lambda/4$-spaced closed contours that the $M = 1$ case requires to suppress interior resonances. For $M > 2$, $M\,\lambda/4$-spaced contour measurements are required in order for (11) to yield an independent set of equations.

A. Condition Number Analysis

The difficulty with combining basis functions from different α-dependent CWEs is that, even if all of the basis functions are mathematically independent, the degree or quality of their independence can be quite poor. We may quantify the independence of these basis functions by reformulating the conjoint CWE as a matrix equation of the form

$$\mathbf{A}\mathbf{x} = \mathbf{b} \tag{13}$$

and calculating the *condition number* κ of the matrix $\mathbf{A}$. In the L-2 norm, the condition number of the matrix $\mathbf{A}$ is equal to the ratio of its largest to smallest singular values $\sigma_{\mathbf{A}}$, as given by [18]

$$\kappa(\mathbf{A}) = \frac{\max(\sigma_{\mathbf{A}})}{\min(\sigma_{\mathbf{A}})}. \tag{14}$$

The singular values of $\mathbf{A}$ are the nonzero elements of the diagonal matrix $\mathbf{S}$ as determined by the SVD of $\mathbf{A}$

$$\mathbf{A} = \mathbf{U}\mathbf{S}\mathbf{V}^H. \tag{15}$$

In (15), $\mathbf{V}^H$ denotes the conjugate transpose of $\mathbf{V}$. The condition number provides a measure of the degree of independence of the matrix columns, with orthogonal matrices having a condition number of one and singular matrices having a condition number of ∞ [18]. For the least squares problem of determining $\mathbf{x}$ from $\mathbf{A}$ and $\mathbf{b}$ in (13), the condition number also relates errors in the solution vector $\mathbf{x}$ to errors in $\mathbf{A}$ and $\mathbf{b}$.

To clarify this relationship and its implications, let us rewrite (11) as a matrix equation of the form in (13). This will require sampling of the electric field E_z at discrete locations along the $\lambda/4$-spaced concentric closed contours surrounding the measurement region. We shall specify a circular region of diameter $D = 10\lambda$ and sample E_z at $\lambda/4$ intervals along each contour. Assuming the far-field condition, this sampling rate corresponds to twice the spatial Nyquist rate. The resulting K measurements at (ρ_i, ϕ_i) form the column vector $\mathbf{b}$. For the case of $M = 1$, we assume K measurements are made along two concentric closed contours in order to suppress interior resonances; for $M > 1$, K measurements are made along M contours. For each allowable wavenumber in the set $\{k_m\}$ defined by (12), the summation with respect to n in (11) is truncated to $-N_m \le n \le N_m$, where N_m is the largest n such that $|n| \le 1.2k_mD/2$. This seemingly arbitrary truncation point was chosen because Bessel functions of order $n > k_mD/2$ show a similar exponentially decaying behavior when evaluated at $\rho \le D/2$ that invariably leads to large condition numbers. The basis functions are then evaluated at the K measurement locations to form the matrix $\mathbf{A}$. The solution vector $\mathbf{x}$ contains the unknown coefficients a_{mn}. Thus, $\mathbf{A}, \mathbf{x}$, and $\mathbf{b}$ are given by

$$\mathbf{A}^T = \begin{bmatrix} J_{-N_1}(k_1\rho_1)e^{-jN_1\phi_1} & \cdots & J_{-N_1}(k_1\rho_K)e^{-jN_1\phi_K} \\ \vdots & \ddots & \vdots \\ J_{N_1}(k_1\rho_1)e^{jN_1\phi_1} & \cdots & J_{N_1}(k_1\rho_K)e^{jN_1\phi_K} \\ J_{-N_2}(k_2\rho_1)e^{-jN_2\phi_1} & \cdots & J_{-N_2}(k_2\rho_K)e^{-jN_2\phi_K} \\ \vdots & \ddots & \vdots \\ J_{N_2}(k_2\rho_1)e^{jN_2\phi_1} & \cdots & J_{N_2}(k_2\rho_K)e^{jN_2\phi_K} \\ \vdots & \vdots & \vdots \\ J_{-N_M}(k_M\rho_1)e^{-jN_M\phi_1} & \cdots & J_{-N_M}(k_M\rho_K)e^{-jN_M\phi_K} \\ \vdots & \ddots & \vdots \\ J_{N_M}(k_M\rho_1)e^{jN_M\phi_1} & \cdots & J_{N_M}(k_M\rho_K)e^{jN_M\phi_K} \end{bmatrix}$$

$$\mathbf{x} = \begin{bmatrix} a_{1,-N_1} \\ \vdots \\ a_{1,N_1} \\ a_{2,-N_2} \\ \vdots \\ a_{2,N_2} \\ \vdots \\ a_{M,-N_M} \\ \vdots \\ a_{M,N_M} \end{bmatrix} \quad \mathbf{b} = \begin{bmatrix} E_z(\rho_1,\phi_1) \\ \vdots \\ E_z(\rho_K,\phi_K) \end{bmatrix}$$

where $\mathbf{A}^T$ denotes the matrix transpose of $\mathbf{A}$.

It is reasonable to expect that the electric field measurements in $\mathbf{b}$ will differ from the actual electric field due to measurement errors stemming from a poor signal-to-noise ratio, interference, and various other system limitations. Let us suppose that the electric field measurement vector $\mathbf{b}$ is given by

$$\mathbf{b} = \mathbf{b_0} + \mathbf{b}_\delta \tag{16}$$

where $\mathbf{b_0}$ represents the true electric field at the measurement locations and $\mathbf{b}_\delta$ is the measurement error. Analogously, let us define the coefficient vector $\mathbf{x}$ as

$$\mathbf{x} = \mathbf{x_0} + \mathbf{x}_\delta \tag{17}$$

where $\mathbf{x_0}$ is the set of coefficients corresponding to the true electric field and $\mathbf{x_\delta}$ is the error in the coefficients due to the measurement error $\mathbf{b_\delta}$. For the linear least squares problem of determining $\mathbf{x}$ from $\mathbf{A}$ and $\mathbf{b}$, the precise relationship between $\mathbf{x_\delta}$ and $\mathbf{b_\delta}$ depends upon how much of the measurement error $\mathbf{b_\delta}$ is described by the column space of $\mathbf{A}$. Without a thorough characterization of the measurement error, a direct relationship is not very useful. However, we are able to define an upper bound on the L-2 norm of $\mathbf{x_\delta}$ using the L-2 norm of $\mathbf{b}_\delta$ [19]

$$||\mathbf{x}_\delta|| \leq \frac{\kappa}{||\mathbf{A}||}||\mathbf{b}_\delta||. \tag{18}$$

In (18), $||\cdot||$ denotes the L-2 norm operator. Equation (18) provides a bound for errors in the basis function coefficients $\mathbf{x}$, but what would be more useful is a bound on the error of the reconstructed field as given by $\mathbf{Ax}$. Using the relation [19]

$$||\mathbf{A}\mathbf{x}_\delta|| \leq ||\mathbf{A}||||\mathbf{x}_\delta|| \tag{19}$$

equation (18) may be rewritten as

$$||\mathbf{A}\mathbf{x}_\delta|| \leq \kappa||\mathbf{b}_\delta||. \tag{20}$$

Thus, we see that, in the worst case, the reconstructed field's error norm $||\mathbf{Ax_\delta}||$ will equal the product of the measurement error's norm $||\mathbf{b_\delta}||$ and the matrix condition number κ. This further indicates that the condition number should be kept small so as to minimize the impact of measurement errors on the accuracy of the reconstructed field. Fig. 2 examines the effect that the wavenumber stepsize Δ has on the condition number of $\mathbf{A}$ when it is compiled from the basis functions of M α-dependent CWEs. Observe that both small wavenumber stepsizes Δ and large M lead to large condition numbers and, thereby, a field reconstruction problem that is very sensitive to measurement error. Small Δ produce sets of α-dependent CWEs with very similar wavenumbers k_m and, thereby, very similar basis functions. When these basis functions are evaluated at discrete locations along the region's closed contours, the matrix $\mathbf{A}$ has columns that are "weakly" independent and result in a large matrix condition number. Increasing the number of allowable k_m by increasing M only serves to compound the problem.

It should be noted that for Fig. 2, the wavenumber stepsize Δ has been normalized by the circular region's diameter D. This accounts for the size of the observation region within which the independence of different basis functions is assessed. In smaller regions, the wavenumber stepsize is a less sensitive parameter and thereby less capable of producing a set of basis functions that are "strongly" independent. As the size of the observation region increases, slight differences in basis functions become more pronounced and the resulting condition number decreases.

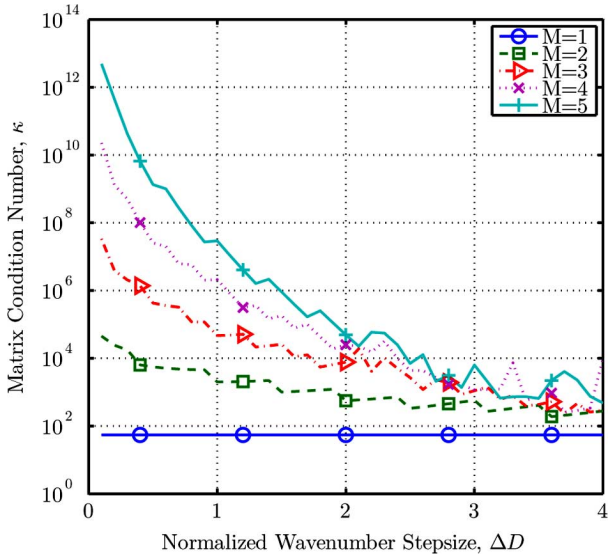

Fig. 2. The matrix condition number indicates that small normalized wavenumber stepsizes ΔD and large numbers of contributing α-dependent CWEs M lead to an ill-conditioned system of equations.

Thus, by normalizing Δ by D, we account for this interrelationship between the wavenumber stepsize, region size, and condition number.

The large condition numbers observed in Fig. 2 may be reduced by simply removing the nearly dependent columns of $\mathbf{A}$. Specifying a maximum condition number $\kappa_{\max}$ and employing (14), we can easily determine the largest set of ℓ singular values that will yield a $\kappa \leq \kappa_{\max}$. Using a subset selection technique based on the QR-decomposition with column pivoting [18, p. 590], we could retain the ℓ "most independent" columns and discard the remainder. However, this technique does not guarantee that the new condition number will be less than $\kappa_{\max}$, although heuristic evidence indicates that this is typically true.

An alternative and more elegant solution employs the SVD to compute a rank ℓ approximation to the pseudoinverse of $\mathbf{A}$ that enables one to directly solve the matrix equation described by (13). Using the SVD, the pseudoinverse of $\mathbf{A}$, denoted $\mathbf{A}^+$, is given by

$$\mathbf{A}^+ = \mathbf{V}\mathbf{S}^+\mathbf{U}^H \tag{21}$$

where $\mathbf{S}^+$ is the pseudoinverse of the diagonal matrix $\mathbf{S}$ [18]. The best rank ℓ approximation to $\mathbf{A}^+$ is given by

$$\mathbf{A}_\ell^+ = \mathbf{V}_\ell\mathbf{S}_\ell^+\mathbf{U}_\ell^H \tag{22}$$

where ℓ is again determined by (14) for some maximum condition number $\kappa_{\max}$, $\mathbf{U}_\ell^H$ and $\mathbf{V}_\ell$ denote the first ℓ rows and columns of $\mathbf{U}^H$ and $\mathbf{V}$, respectively, and $\mathbf{S}_\ell^+$ is the upper leftmost ℓ-by-ℓ submatrix of $\mathbf{S}^+$. This rank ℓ approximation matrix may then be used directly to solve for the coefficient vector $\mathbf{x}$ in (13)

$$\mathbf{x}_\ell = \mathbf{b}\mathbf{A}_\ell^+. \tag{23}$$

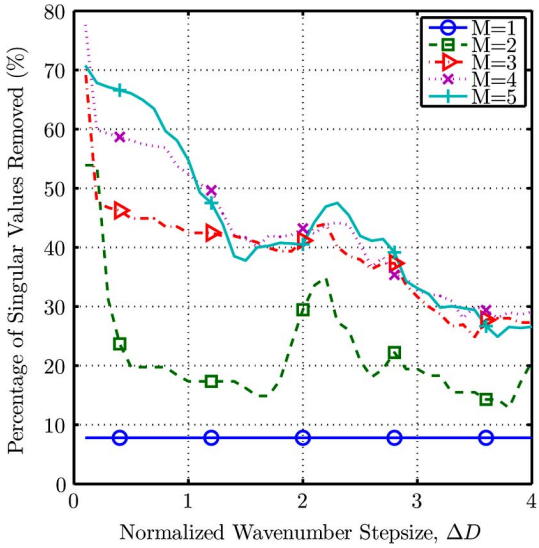

Fig. 3. The percentage of singular values that must be removed from the basis function matrix $\mathbf{A}$ to attain a condition number κ less than ten for various M.

Here, $\mathbf{x}_\ell$ indicates that the coefficient vector is computed using $\mathbf{A}_\ell^+$ as opposed to the actual pseudoinverse. By using the rank ℓ approximation to $\mathbf{A}^+$, the condition number amplifying the measurement error in (18) and (20) is guaranteed to be at most $\kappa_{\max}$.

It should be recognized, however, that by removing small singular values, the coefficient vector $\mathbf{x}_\ell$ is not fully utilizing the entire column space of $\mathbf{A}$ to solve the matrix equation problem in (13). Let us specify a maximum condition number of $\kappa_{\max} = 10$ and examine the percentage of singular values that must be removed to construct the rank ℓ approximation to $\mathbf{A}^+$. Using (20), we note that in the worst case, a $\kappa_{\max} = 10$ would lead to a reconstructed field error norm that is ten times the measurement error norm. Considering this represents the *worst case-scenario,* we expect that $\kappa_{\max} = 10$ will be acceptable for most situations.

Fig. 3 compares the percentage of singular values removed from $\mathbf{A}$ to attain a $\kappa \leq 10$ for various M. Note that even the $M = 1$ case corresponding to the conventional CWE required that singular values be removed. This provides further justification for truncating (11)'s summation with respect to n such that $|n| \leq 1.2k_m D/2$: including basis functions corresponding to $|n| > 1.2k_m D/2$ has very little effect on the construction of the rank ℓ approximation to $\mathbf{A}^+$. For $M > 2$, we observe that a large percentage of the singular values were removed. Also, note that for $M = 2$ in the range $0.5 \leq \Delta D \leq 1.5$, less than 20% of the singular values were removed to attain a $\kappa \leq 10$. Similar analysis for diameters ranging from $D = 2\lambda$ to $D = 50\lambda$ indicates that this behavior is independent of the region's diameter.

Recall that as we increase the number of contributing α-dependent CWEs by raising M, we require knowledge of E_z along additional closed contours to ensure a uniquely solvable set of equations. Thus, large M require more time-consuming measurements, and yet, according to Fig. 3, they do not significantly affect the composition of $\mathbf{A}_\ell^+$. Therefore, it seems that increasing M is not a very efficient means to developing an accurate expansion for quasi 2-D fields. Based on this analysis, we shall specify henceforth that $M = 2$. Thereby, the conjoint CWE requires the same two measurement contours as the conventional CWE while hopefully providing a more accurate field reconstruction for some chosen Δ.

B. Accuracy Analysis

To determine the appropriate wavenumber stepsize Δ for the conjoint CWE in (11), the accuracy of the expansion was evaluated within a circular region of diameter D. The electric field due to a single homogeneous plane wave with a wavevector given by the angle pair $(\beta = 0, \alpha)$ was sampled at $\lambda/4$ intervals along two $\lambda/4$-spaced concentric circular contours. Specifying $M = 2$ for the conjoint CWE described in (11) and a maximum condition number $\kappa_{\max} = 10$, the matrix equation was solved by way of (23) for the coefficient vector $\mathbf{x}_\ell$. Then, (11) was used to reconstruct the field within the circular region. The *reconstruction error* was defined as the magnitude difference between the reconstructed complex electric field and the true complex field.

Fig. 4(a) and (b) presents the mean-squared reconstruction error, denoted ε^2, for circular regions of diameter 5λ and 10λ, respectively. Note that the curves denoted by $\Delta D = 0$ correspond to the conventional CWE given by (1). Effectively, the expansions seek to approximate a plane wave of wavenumber $k\cos\alpha$ to a plane wave of wavenumber k_m. Thus, as k_m approaches $k\cos\alpha$, we observe a null in the reconstruction error that indicates an accurate approximation. More so, when observed over increasingly larger regions, errors in the approximation of $k\cos\alpha$ by k_m become more apparent because the approximation's phase error grows linearly with distance. Thereby, smaller diameter regions tend to have smaller reconstruction errors, as evidenced by a comparison of Fig. 4(a) and (b).

As α approaches 0°, we observe that ε^2 falls below 10^{-3} for both CWEs. For practical applications, this small reconstruction error is negligible, especially in comparison to the error incurred by the conventional CWE for plane waves incident at relatively small elevation angles. The conjoint CWE's nonzero ΔD is seen to significantly reduce the reconstruction error for small α; however, if ΔD is too large, the accuracy of the conjoint CWE actually becomes worse than the conventional CWE. From Fig. 3, we determined that for $M = 2$, the wavenumber stepsize should be such that $0.5 \leq \Delta D \leq 1.5$ to minimize the number of nearly dependent basis functions. Here, we see that this bound might be further restricted to $0.5 \leq \Delta D \leq 1$ to ensure the conjoint CWE's reconstruction error is less than the conventional CWE's for quasi-2-D fields characterized by small α. Thus, formally, we conclude that, for a circular region of diameter D, the conjoint CWE's wavenumber stepsize should be such that

$$\frac{1}{2D} \leq \Delta \leq \frac{1}{D}. \tag{24}$$

This allows the wavenumber stepsize to be optimized for a given propagation environment. If plane waves incident at large elevation angles are expected to contribute to the measured fields, a Δ nearer to $1/D$ would be preferable; if the AoAs are expected

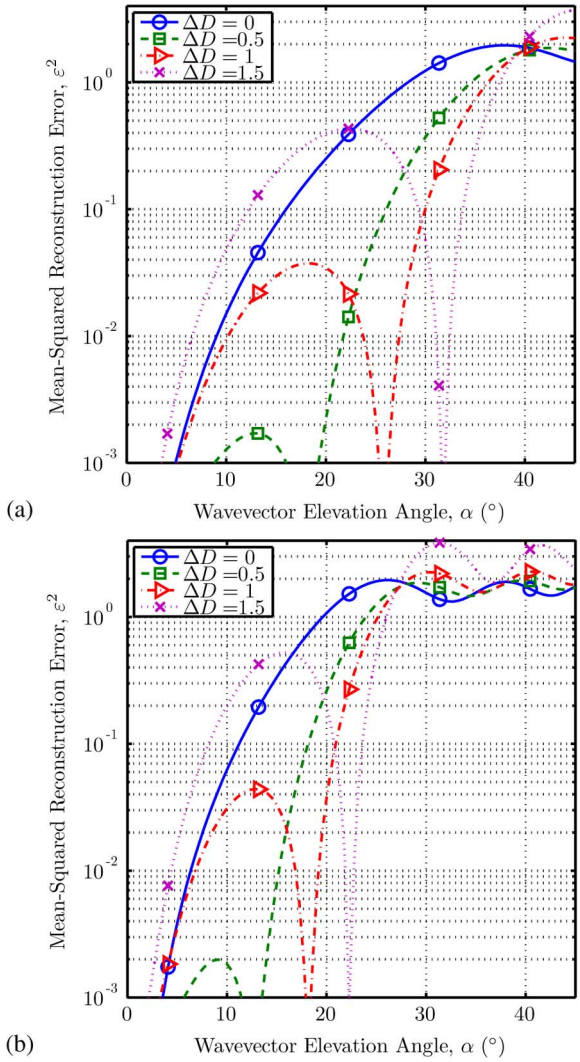

Fig. 4. The conjoint CWE's mean-squared reconstruction error ε^2 for a single plane wave propagating with a wavevector elevation angle α across a circular region of diameter D with $M = 2$ and $\kappa_{\max} = 10$: (a) $D = 5\lambda$ and (b) $D = 10\lambda$. $\Delta D = 0$ corresponds to the conventional CWE.

to cluster tightly about the horizon, then a Δ of $1/(2D)$ would likely perform best.

V. Analytical Field Reconstruction Error

It is elucidating to consider the continuous form of the field reconstruction problem wherein the field is reconstructed from *continuous* field measurements along a pair of concentric closed contours. Let us analytically determine the mean-squared error ε^2 of the conventional and conjoint CWEs for an arbitrary electric field $E(\vec{r})$ given by

$$E(\vec{r}) = \sum_{i=1}^{N} E_{0,i} e^{j\Phi_i} e^{-jk\rho\cos\alpha_i\cos(\beta_i-\phi)} \tag{25}$$

throughout a circular region Ω of radius $\rho_0 = D/2$ provided a pair of concentric circular measurement contours Γ at radii $\rho = \{\rho_0, \rho_0'\}$ with $\rho_0' = \rho_0 - \lambda/4$. Equation (25) describes the field due to N plane waves, each with a magnitude $E_{0,i}$, complex phase $e^{j\Phi_i}$, real wavevector elevation angle α_i, and arbitrary wavevector azimuth angle β_i. Generally, the problem is to compute

$$\varepsilon^2 = \frac{L_2\{E(\vec{r}) - A(\vec{r})\}_\Omega^2}{\pi\rho_0^2} \tag{26}$$

where $L_2\{(\cdot)\}_\Omega$ is the continuous L-2 norm operator given by [20]

$$L_2\{(\cdot)\}_\Omega = \left[\int_\Omega |(\cdot)|^2 d\Omega\right]^{1/2} \tag{27}$$

and $A(\vec{r})$ is the conventional or conjoint CWE given by

$$A(\vec{r}) = \sum_n f_n(\rho) e^{jn\phi} \tag{28}$$

where

$$f_n(\rho) = \begin{cases} b_n J_n(k\rho), & \text{for } \Delta D = 0 \\ c_n J_n(k\rho) + d_n J_n(k'\rho), & \text{for } \Delta D \neq 0 \end{cases} \tag{29}$$

and $k' = k - \pi\Delta$, which corresponds to k_2 in (12). The coefficients b_n (for $\Delta D = 0$) or c_n and d_n (for $\Delta D \neq 0$) are determined from the minimization problem

$$\min L_2\{E(\vec{r}) - A(\vec{r})\}|_{\vec{r}\in\Gamma} \tag{30}$$

along the two measurement contours Γ. We note that an analytical expression may be found for ε^2, but its application requires explicit knowledge of Φ_i. A simpler and more practical solution may be found by assuming that (25) describes *uncorrelated scattering* and deriving the *expected value* of ε^2. Uncorrelated scattering assumes that Φ_i is a random variable realized from a probability density function uniformly distributed from zero to 2π and

$$\mathrm{E}\{e^{j(\Phi_p - \Phi_q)}\} = \begin{cases} 1, & \text{for } p = q \\ 0, & \text{for } p \neq q \end{cases} \tag{31}$$

where $\mathrm{E}\{(\cdot)\}$ denotes the expected value (or ensemble average) of $(\cdot)$ [21]. The expected value of ε^2 is then given by

$$\overline{\varepsilon^2} = \mathrm{E}\left\{\frac{L_2\{E(\vec{r}) - A(\vec{r})\}_\Omega^2}{\pi\rho_0^2}\right\}. \tag{32}$$

Physically, (31) implies that each of the incident waves arises due to different scattering mechanisms [22]. Given the complexity of real-world propagation environments, this is generally considered to be a sound assumption.

A rigorous, albeit highly compressed, analysis in the Appendix illustrates how $\overline{\varepsilon^2}$ may be derived for both the conventional and conjoint CWEs for an electric field described by (25). Consideration of these analytical solutions provides powerful insight for applying both the conventional and conjoint

CWEs to real-world field reconstruction problems. We first note that (41) and (44), which describe the mean-squared reconstruction error for a single unit amplitude plane wave, are in exact agreement with the simulation-based error curves plotted in Fig. 4. This lends confidence to the analytical expressions in the Appendix as well as the numerical implementation of the conjoint CWE described in Section IV.

Secondly, we observe from (41) and (44) that the mean-squared reconstruction error for the field due to a single, unit amplitude plane wave, denoted ε_0^2, is independent of both the wave's phase and azimuth AoA. Therefore, although the error curves in Fig. 4 were generated for the specific case of a unit amplitude homogeneous plane wave having $\beta = 0$, they are applicable to any unit amplitude plane wave including inhomogeneous plane waves provided that the wavevector elevation angle α is real.

For the arbitrary field described by (25), provided that the uncorrelated scattering assumption holds, the expected value of ε^2 is given by

$$\overline{\varepsilon^2} = \sum_{i}^{N} E_{0,i}^2 \varepsilon_0^2(\alpha_i). \tag{33}$$

Equation (33) reveals that $\overline{\varepsilon^2}$ is just a summation of the α-dependent mean-squared reconstruction errors for the N plane waves, with each $\varepsilon_0^2(\alpha_i)$ weighted by the corresponding waves's power, $E_{0,i}^2$. Therefore, provided an elevation power angle spectrum $p(\theta)$, the uncorrelated scattering assumption, and ε_0^2 for either the conventional or conjoint CWE, $\overline{\varepsilon^2}$ is also given by

$$\overline{\varepsilon^2} = \int_{-\pi/2}^{\pi/2} \varepsilon_0^2(\alpha) p(-\alpha) d\alpha. \tag{34}$$

In practice, it may be more convenient to work with a power-normalized form of the total mean squared error

$$\widehat{\overline{\varepsilon^2}} = \frac{\int_{-\pi/2}^{\pi/2} \varepsilon_0^2(\alpha) p(-\alpha) d\alpha}{\int_{-\pi/2}^{\pi/2} p(-\alpha) d\alpha}. \tag{35}$$

This formulation allows for comparison of reconstruction errors between measurement sites with different total received powers. The approximate power angle spectrum $p(\theta)$ may be determined from the perimeter measurement data using Fourier-based beamsteering techniques, though this approach will invariably overestimate the error due to the planar array geometry's large beamwidth in elevation. Alternatively, $p(\theta)$ may be determined from ray-based propagation prediction techniques or from statistical distributions of power versus elevation for specific propagation environments. The latter two approaches are particularly useful for predicting reconstruction errors during the planning stages of a measurement campaign.

VI. Experimental Validation

As a final validation and demonstration of the utility of the proposed technique, the conjoint CWE was applied to field measurements obtained near the corner of an exterior wall composed of brick on the outside and cinder block on the inside. Fig. 5(a) diagrams the measurement area photographed in Fig. 5(b). The measurement area comprised the fifth floor of an academic building as well as the gravel roof atop the fourth floor. Note that the fifth floor occupies a fraction of the building's full footprint and thereby allowed access to the fourth floor roof. Also, we note that the gravel rooftop made for an electromagnetically rough surface that likely scattered the coherent specular ground reflection into diffuse waves with slightly negative elevation AoAs.

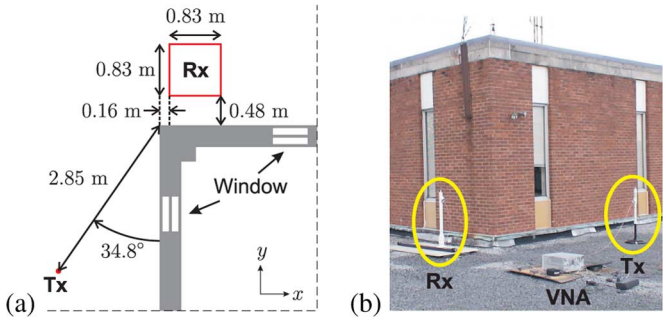

Fig. 5. Using a VNA, S_{21} measurements were made on a 28 by 28 point measurement grid near the corner of an exterior wall. Rx denotes the receiver measurement grid and Tx the transmitter. (a) Overhead diagram and (b) photo of measurement.

A vector network analyzer (VNA) and linear positioner were used to make S_{21} measurements of the 2.45 GHz industrial, scientific, and medical band wireless channel. For a static channel and a fixed transmitter, complex S_{21} measurements are directly proportional to the time-harmonic electric field. Both the transmit and receive antennas were vertically polarized quarter-wavelength monopole antennas mounted atop a 1.15 m polyvinyl chloride mast. The receive antenna's mast was attached to the linear positioner, which had a position accuracy of 1×10^{-5}m; the transmit antenna's mast was attached to a stationary stand. A 2.45 GHz bandpass filter and 10 ft coaxial cable was connected to ports 1 and 2 of the VNA. Following a two-port calibration, the cable ends were connected to the antennas. For each measurement location, the VNA was swept from 2.4 to 2.488 GHz in 1 MHz increments. Measurements were taken at $\lambda/4$ intervals on a rectangular grid that measured 6.75λ by 6.75λ, with $\lambda = 0.1224$ m corresponding to the free-space wavelength at 2.45 GHz. Temporal averaging of measurement data minimized the effect of time-varying scatterers. Fig. 6(a) shows the magnitude and phase of the measured S_{21} at 2.45 GHz in decibels (dB) and degrees, respectively. For comparison, Fig. 7(b) presents the corresponding uniform theory of diffraction (UTD) solution for a unit amplitude plane wave incident on a perfectly electrically conducting 90° wedge. Observe that there is good agreement between the S_{21} measurements and the ideal UTD solution.

Using only perimeter S_{21} data corresponding to the measurement grid's two outermost rectangular contours, the S_{21} was reconstructed within the rectangular measurement region using the conjoint CWE with select normalized wavenumber stepsizes ΔD. The diameter D was set to the length of the measurement region's diagonal $D = \sqrt{2} \cdot 6.75\lambda$. Fig. 7 presents the error

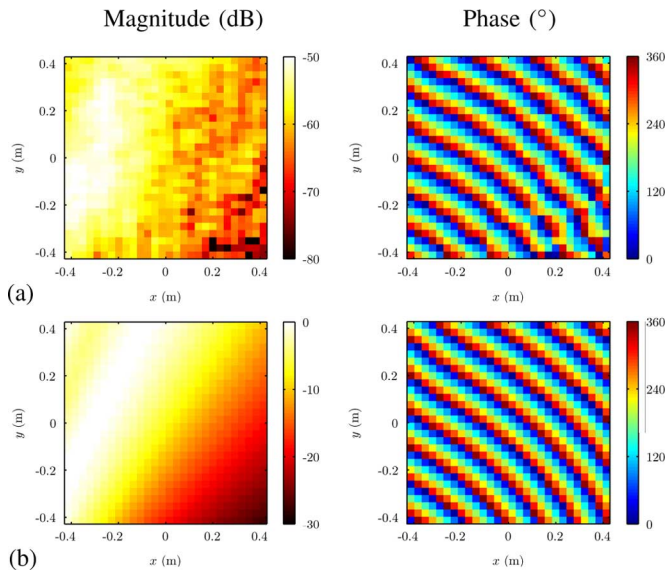

Fig. 6. The magnitude (dB) and phase (°) of S_{21} for the diffraction measurement setup at 2.45 GHz: (a) the measured S_{21} and (b) the ideal UTD-based calculation.

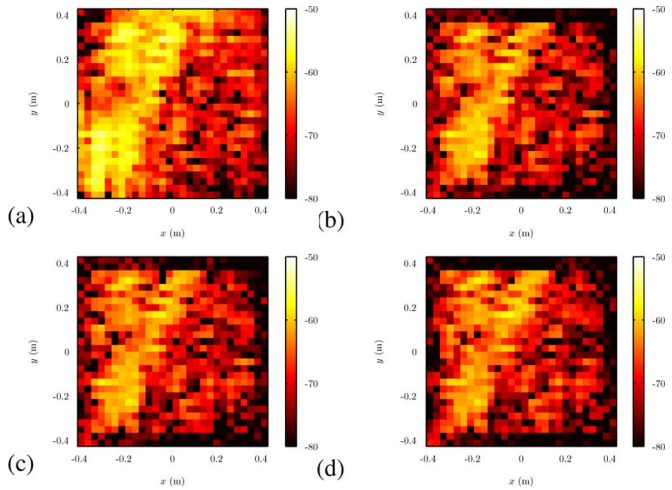

Fig. 7. Spatial error maps for the reconstructed S_{21} in dB at 2.45 GHz for select wavenumber stepsizes: (a) $\Delta D = 0$, (b) $\Delta D = 1/2$, (c) $\Delta D = 3/4$, and (d) $\Delta D = 1$.

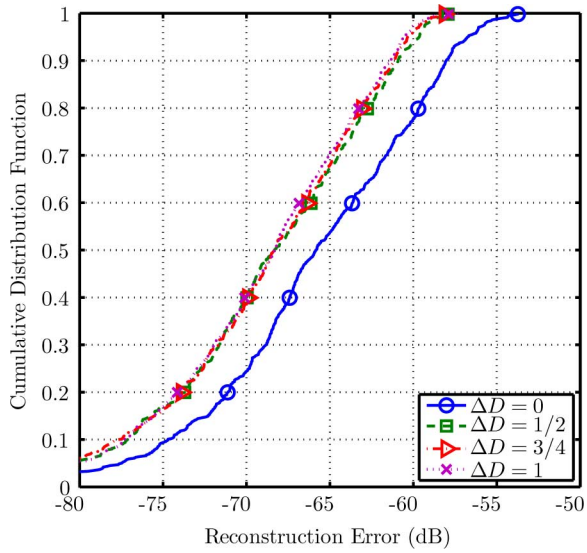

Fig. 8. A comparison of the error cumulative distribution functions for the reconstructed S_{21} in the measurement region's "interior" at 2.45 GHz.

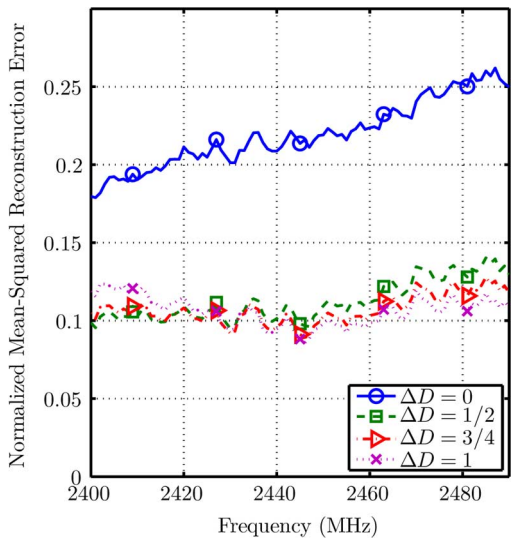

Fig. 9. Normalized mean-squared reconstruction error in the measurement region's "interior" for $\Delta D = \{0, 1/2, 3/4, 1\}$.

(dB) of the reconstructed S_{21} at 2.45 GHz. The reconstruction error was calculated as the magnitude of the difference between the measured and reconstructed S_{21}. Note that the error maps in Fig. 7 have been drawn with the same dB colormap as the measured S_{21} magnitude presented in Fig. 6(a) so as to facilitate comparisons. This allows us to observe that although the reconstruction error tends to follow the magnitude of the measured S_{21}, the reconstruction error is generally smaller. Overall, we find that the conjoint CWEs ($\Delta D \neq 0$) have a smaller reconstruction error than the conventional CWE ($\Delta D = 0$). Significant improvements are observed near the region's perimeter, as might be expected given the conjoint CWE's larger set of basis functions. To better compare the accuracy of the conjoint and conventional CWEs, cumulative distribution function (cdf) error curves were calculated from the *interior* of the rectangular region. By "interior" we refer to the measurement sites bounded by the two outer closed contours and thereby exclude the perimeter points where the conjoint CWEs showed substantial error reductions so as to more fairly compare the error cdfs. Fig. 8 presents the resulting cdfs. Despite excluding the perimeter region for which the conjoint CWE showed significant gains, we still observe that the conjoint CWE ($\Delta D \neq 0$) reduces both the ninety-fifth percentile and maximum reconstruction error by at least 3 dB.

Fig. 9 examines the mean-squared reconstruction error throughout the "interior" region as a function of frequency. The mean-squared reconstruction error at each frequency was normalized by the interior's mean-squared S_{21}. As Fig. 9 shows, the conjoint CWEs yielded consistently smaller reconstruction errors across the entire measurement band. The overall trend of increasing error with frequency is attributed to the increasing electromagnetic size of the measurement region. At higher frequencies, the electromagnetic size of the region is larger,

leading to larger reconstruction errors as suggested by the error curves in Fig. 4.

VII. Conclusion

For the quasi-2-D fields encountered in real-world wireless channels, the conjoint CWE essentially offers something for nothing. Using the same pair of measurement contours, both analytical and empirical data indicate that the conjoint CWE provides significant reductions in field reconstruction error compared to the conventional CWE. Thereby, the conjoint CWE allows one to more accurately analyze the electromagnetic fields within a planar region while incurring no additional measurement overhead. As the diffraction measurements presented here indicate, this improved accuracy makes expansion-based field reconstruction a viable alternative to measuring the channel throughout a planar region. Rather than tediously measuring the field everywhere, one only requires measurements along a pair of perimeter contours. This order-of-magnitude reduction in measurement time coupled with the improved field reconstruction accuracy of the conjoint CWE will at long last enable a measurement-based investigation of real-world propagation mechanisms.

Appendix I
Conventional CWE's Mean-Squared Error

Using (8), (25) becomes

$$E(\vec{r}) = \sum_{i=1}^{N} \sum_{n} a_{n,i} J_n(k\rho \cos \alpha_i) e^{jn\phi} \tag{36}$$

where the coefficient $a_{n,i}$ is given by

$$a_{n,i} = E_{0,i} e^{j\Phi_i} e^{jn(\beta_i - \pi/2)}. \tag{37}$$

Substituting (36) and (37) into (26) and evaluating the L-2 norm yields

$$\begin{aligned} & L_2\{E(\vec{r}) - A(\vec{r})\}^2|_{\vec{r}\in\Gamma} \\ & = 2\pi \sum_{n} \Bigg[\rho_0 |b_n|^2 J_n^2(k\rho_0) + \rho_0' |b_n|^2 J_n^2(k\rho_0') \\ & -\rho_0 \sum_{i=1}^{N} (a_{n,i} b_n^* + a_{n,i}^* b_n) J_n(k\rho_0) J_n(k\rho_0 \cos\alpha_i) \\ & -\rho_0' \sum_{i=1}^{N} (a_{n,i} b_n^* + a_{n,i}^* b_n) J_n(k\rho_0') J_n(k\rho_0' \cos\alpha_i) \\ & +\rho_0 \sum_{p=1}^{N} \sum_{q=1}^{N} a_{n,p} a_{n,q}^* J_n(k\rho_0 \cos\alpha_p) J_n(k\rho_0 \cos\alpha_q) \\ & +\rho_0' \sum_{p=1}^{N} \sum_{q=1}^{N} a_{n,p} a_{n,q}^* J_n(k\rho_0 \cos\alpha_p) J_n(k\rho_0' \cos\alpha_q) \Bigg]. \end{aligned} \tag{38}$$

The coefficient b_n that minimizes (38) is found to be

$$b_n = \sum_{i=1}^{N} \chi_n^b(\alpha_i) a_{n,i} \tag{39}$$

where

$$\begin{aligned} & \chi_n^b(\alpha) \\ & = \frac{\rho_0 J_n(k\rho_0 \cos\alpha) J_n(k\rho_0) + \rho_0' J_n(k\rho_0' \cos\alpha) J_n(k\rho_0')}{\rho_0 J_n^2(k\rho_0) + \rho_0' J_n^2(k\rho_0')}. \end{aligned} \tag{40}$$

Solving (32) with the minimizing coefficient and the aid of [23] yields the expected value of the mean-squared error given in (33), where $\varepsilon_0^2(\alpha)$ may be shown to be the mean-squared error due to a single, unit amplitude plane wave propagating at a wavevector elevation angle α as given by

$$\begin{aligned} & \varepsilon_0^2(\alpha) \\ & = 1 + \sum_{n} \left[\left(\chi_n^b(\alpha)\right)^2 F_n(k) - 4\chi_n^b(\alpha) G_n(k, k\cos\alpha) \right] \end{aligned} \tag{41}$$

and F_n and G_n are helper functions defined as

$$\begin{aligned} & F_n(k) \\ & = \left[J_n^2(k\rho_0) - J_{n-1}(k\rho_0) J_{n+1}(k\rho_0) \right] \end{aligned} \tag{42}$$

$$\begin{aligned} & G_n(k_1, k_2) \\ & = \frac{k_2 J_{n-1}(k_2\rho_0) J_n(k_1\rho_0) - k_1 J_{n-1}(k_1\rho_0) J_n(k_2\rho_0)}{\rho_0 \left(k_1^2 - k_2^2\right)}. \end{aligned} \tag{43}$$

Appendix II
Conjoint CWE's Mean-Squared Error

Through similar albeit more tedious mathematical manipulations, one may determine that $\overline{\varepsilon^2}$ for the conjoint CWE is again given by (33), where the unit amplitude plane wave's mean-squared error is given by

$$\begin{aligned} & \varepsilon_0^2(\alpha) \\ & = 1 + \sum_{n} \Big[\left(\chi_n^c(\alpha)\right)^2 F_n(k) + \left(\chi_n^d(\alpha)\right)^2 F_n(k') \\ & \quad -4\chi_n^c(\alpha) G_n(k, k\cos\alpha) - 4\chi_n^d(\alpha) G_n(k', k\cos\alpha) \\ & \quad +4\chi_n^c(\alpha)\chi_n^d(\alpha) G_n(k, k') \Big] \end{aligned} \tag{44}$$

$$\begin{aligned} & \chi_n^c(\alpha) \\ & = \frac{J_n(k'\rho_0') J_n(k\rho_0\cos\alpha) - J_n(k'\rho_0) J_n(k\rho_0'\cos\alpha)}{J_n(k\rho_0) J_n(k'\rho_0') - J_n(k'\rho_0) J_n(k\rho_0')} \end{aligned} \tag{45}$$

$$\begin{aligned} & \chi_n^d(\alpha) \\ & = \frac{J_n(k\rho_0') J_n(k\rho_0\cos\alpha) - J_n(k\rho_0) J_n(k\rho_0'\cos\alpha)}{J_n(k'\rho_0) J_n(k\rho_0') - J_n(k\rho_0) J_n(k'\rho_0')}. \end{aligned} \tag{46}$$

The minimizing coefficients are given by

$$c_n = \sum_{i=1}^{N} a_{n,i} \chi_n^c(\alpha_i) \tag{47}$$

$$d_n = \sum_{i=1}^{N} a_{n,i} \chi_n^d(\alpha_i). \tag{48}$$

REFERENCES

[1] W. C.-Y. Lee, "The elevation angle of mobile radio signal arrival," *IEEE Trans. Commun.*, vol. COM-21, pp. 1194–1197, Nov. 1973.

[2] J. Laurila, K. Kalliola, M. Toeltsch, K. Hugl, P. Vainikainen, and E. Bonek, "Wide-band 3-D characterization of mobile radio channels in urban environment," *IEEE Trans. Antennas Propag.*, vol. 50, pp. 233–243, Feb. 2002.

[3] A. Kuchar, J.-P. Rossi, and E. Bonek, "Directional macro-cell channel characterization from urban measurements," *IEEE Trans. Antennas Propag.*, vol. 48, pp. 137–146, Feb. 2000.

[4] K. Kalliola, H. Laitinen, P. Vainikainen, M. Toeltsch, J. Laurila, and E. Bonek, "3-D double-directional radio channel characterization for urban macrocellular applications," *IEEE Trans. Antennas Propag.*, vol. 51, pp. 3122–3133, Nov. 2003.

[5] N. Blaunstein, M. Toeltsch, C. G. Christodoulou, J. Laurila, E. Tsalolihin, E. Bonek, P. Vainikainen, N. Tsouri, K. Kalliloa, and H. Laitinen, "Azimuth, elevation, and time-delay distributions in wireless communication channels," *IEEE Antennas Propag. Mag.*, vol. 48, pp. 160–167, Feb. 2006.

[6] N. Blaunstein, M. Toeltsch, J. Laurila, E. Bonek, D. Katz, P. Vainikainen, N. Tsouri, K. Kalliola, and H. Laitinen, "Signal power distributions in the azimuth, elevation and time delay domains in urban environments for various elevations of base station antenna," *IEEE Trans. Antennas Propag.*, vol. 54, pp. 2902–2916, Oct. 2006.

[7] K. Kalliola, K. Sulonen, H. Laitinen, O. Kivekäs, J. Krogerus, and P. Vainikainen, "Angular power distribution and mean effective gain of mobile antenna in different propagation environments," *IEEE Trans. Veh. Technol.*, vol. 51, pp. 823–838, Sep. 2002.

[8] O. Landron, M. J. Feuerstein, and T. S. Rappaport, "A comparison of theoretical and empirical reflection coefficients for typical exterior wall surfaces in a mobile radio environment," *IEEE Trans. Antennas Propag.*, vol. 44, pp. 341–351, Mar. 1996.

[9] C. L. Dillard, T. M. Gallagher, C. W. Bostian, and D. G. Sweeney, "Rough surface scattering from exterior walls at 28 GHz," *IEEE Trans. Antennas Propag.*, vol. 52, pp. 3173–3179, Dec. 2004.

[10] Y. I. Nechayev, C. C. Constantinou, and L. Lukama, "Comparison of measured and theoretical diffracted fields around building corners at 2.4 GHz," in *Proc. IEEE VTS 54th Veh. Technol. Conf. 2001*, Oct. 7–11, 2001, vol. 2, pp. 728–732.

[11] M. Ghoraishi, J. Takada, and T. Imai, "Identification of scattering objects in microcell urban mobile propagation channel," *IEEE Trans. Antennas Propag.*, vol. 54, pp. 3473–3480, Nov. 2006.

[12] J.-P. Rossi, J. Wiart, and F. Eynard, "In situ measurement of reflection and diffraction coefficients of UHF radio waves on buildings using a ring array," *Radio Sci.*, vol. 35, no. 2, pp. 361–369, Mar. 2000.

[13] J.-P. Rossi, J.-P. Barbot, and A. J. Levy, "Theory and measurement of the angle of arrival and time delay of UHF radiowaves using a ring array," *IEEE Trans. Antennas Propag.*, vol. 45, pp. 876–884, May 1997.

[14] J. A. Stratton, *Electromagnetic Theory*, 1st ed. New York: McGraw-Hill, 1941.

[15] A. F. Peterson, "The interior resonance problem associated with surface integral equations of electromagnetics: Numerical consequences and a survey of remedies," *Electromagnetics*, vol. 10, no. 3, pp. 293–312, 1990.

[16] M. B. Woodworth and A. D. Yaghjian, "Derivation, application conjugate gradient solution of the dual-surface integral equations for three-dimensional, multi-wavelength perfect conductors," in *PIER 5: Progress in Electromagnetics Research*, T. Sarkar, Ed. New York: Elsevier, 1991, pp. 103–130.

[17] R. A. Shore and A. D. Yaghjian, "Dual-surface integral equations in electromagnetic scattering," *IEEE Trans. Antennas Propag.*, vol. 53, pp. 1706–1709, May 2005.

[18] G. H. Golub and C. F. Van Loan, *Matrix Computations*. Baltimore, MD: Johns Hopkins Univ. Press, 1983.

[19] C. L. Lawson and R. J. Hanson, *Solving Least Squares Problems*. Englewood Cliffs, NJ: Prentice-Hall, 1974.

[20] J. R. Rice, *The Approximation of Functions*. Reading, MA: Addison-Wesley, 1964.

[21] A. Papoulis, *Probability, Random Variables, and Stochastic Processes*. : McGraw-Hill, 1965.

[22] G. D. Durgin, *Space-Time Wireless Channels*. Upper Saddle River, NJ: Prentice-Hall, 2003.

[23] I. S. Gradshteyn and I. M. Ryzhik, *Table of Integrals, Series, and Products*, A. Jeffrey and D. Zwillinger, Eds. San Diego, CA: Academic, 2000.

Ryan J. Pirkl (S'04) received the B.S. and M.S. degrees in electrical engineering from the Georgia Institute of Technology, Atlanta, in 2005 and 2007, respectively, where he is currently pursuing the Ph.D. degree in electrical engineering.

His studies include in situ measurement techniques for characterizing radio wave propagation mechanisms. His research interests are radio wave propagation, radio-frequency engineering, and analytical electromagnetics.

Gregory D. Durgin (S'96–M'01–SM'06) received the B.S.E.E., M.S.E.E., and Ph.D. degrees from Virginia Polytechnic Institute and State University, Blacksburg, in 1996, 1998, and 2000, respectively.

He joined the Department of Electrical and Computer Engineering, Georgia Institute of Technology (Georgia Tech), Atlanta, as an Assistant Professor in 2003. His primary research areas are radio wave propagation, radiolocation, and applied electromagnetics. In 2001, he received a Japanese Society for the Promotion of Science Postdoctoral Fellowship and spent one year as a Visiting Researcher with Morinaga Laboratory, Osaka University, Japan. He is the author of *Space-Time Wireless Channels* (Upper Saddle River, NJ: Prentice-Hall, 2003), the first textbook in the field of space–time channel modeling.

In 1998, Prof. Durgin received (with T. S. Rappaport and H. Xu) the Stephen O. Rice Prize for best original journal article in the IEEE TRANSACTIONS ON COMMUNICATIONS. He has won numerous teaching awards at Georgia Tech.